Production of Plated Girders: Geometry, Geometric Imperfections and Residual Stresses

Sebastião Gomes Ferreira
sebastiao.o.a.gomes.ferreira@tecnico.ulisboa.pt

Abstract

The competitiveness of steel structures depends on effective material use. Reduce the thickness of the plates used in plate girders, especially those of the stiffened webs, result in plates with extremely high slenderness. However, these design options must be evaluated in combination with the production requirements, both in terms of respecting to geometric tolerances and avoid introducing high residual stresses during the production process.

However, the effects of the thermal methods used to produce plate girders, which result in the introduction of residual stresses and geometric imperfections in the beam cross-sections, have usually a secondary significance. In reality, even if these effects are taken into indirect consideration during safety verifications, they may still influence whether or not the plate girders are accepted to be used, which may result in additional repair costs or even the replacement of defective beams.

This study examines the stages of the production of slender steel plate girders, collecting experimentally the geometric imperfections and residual stresses resulting from the cutting and welding processes of two beams, and numerically reproducing the same production operations.

The results match in terms of residual stresses and geometrical imperfections for the separate effects of thermal cut and welding processes. The study attempt to combine with the effects of plate cutting and web-to-flange welding in order to understand the impact of each stage of production on the final plate girder outcome.

Keywords: Residual stresses; Geometric imperfections; Thermal cut; Welding process; Finite elements model; Plate slenderness.

1. Introduction

Welded section beams, due to its competitive design, must endure several thermal processes in its production, this means that some effects that could not be considered in other types of structural elements now have to be considered with special attention.

The present study is based on the production results of 8 beams and 4 stages of production: The thermal cut of the web and flange plates, the welding of the flange-web joint, the cold cut of the beam, and the welding of the transverse stiffeners. It is also important to refer that the beam have a steel grade S355.

The main purpose of this work was to show how each step influences the final residual stresses and geometric imperfections of the beam. It was also another goal to find a way of adding each step effect in the final residual stresses field to be acceptable considering each stage effect as an isolated outcome.

2. State of the art

2.1. Residual stresses

All the stages of plate girders production are responsible for the development of residual stresses or geometric imperfections. Such phenomenon, such as the occurrence of residual stresses occurs due to the following theoretical concept.

When we have an object at an initial equilibrium temperature (e.g. 21°C) and the object's temperature is very much increased in a specific area then some auto-equilibrated reactions will have to appear in the object, so it can remain in equilibrium. This theoretical conception can be observed in the Figure 1 .

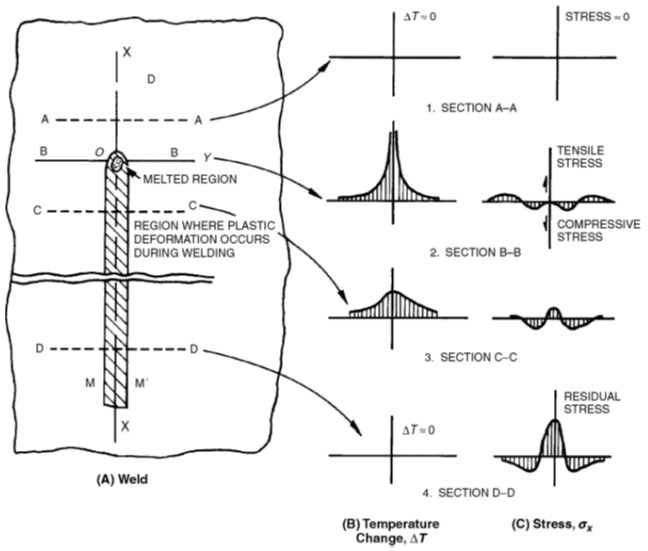

Figure 1– Residual stresses due to a welded region [2]

It can also be seen that the stresses after the object's cooling won't be the same that were there before the process. In fact, there will be a gradient of temperature in the cooling of the body that will force the object to generate a permanent stress field, known as a residual stress field [1-4].

However, is important to refer that the residual stresses field showed in Figure 1 considers only one thermal action applied in a stressless plate. Considering that, in the case of the present investigation, it will be studied several thermal actions in different positions of the object, the stress field can show a different shape. In a similar study of the "Universidade de Coimbra", the shape of the residual stresses were as presented below.

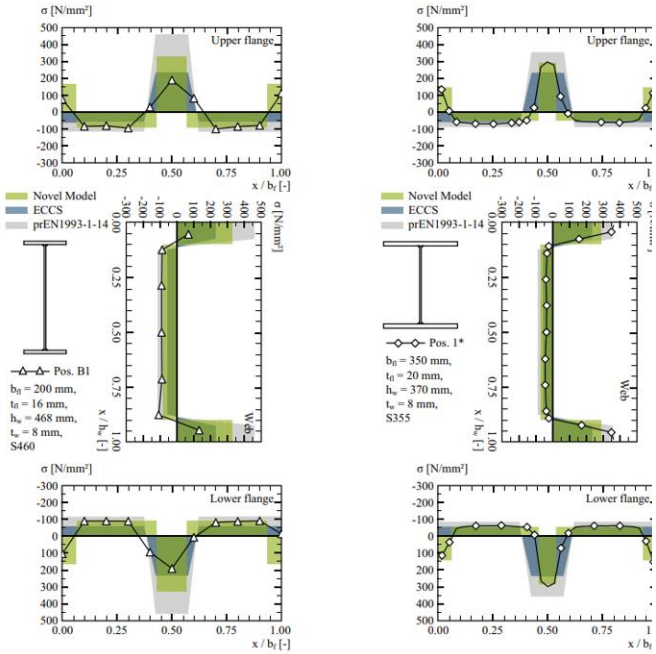

Figure 2– Combined residual stresses field due to the thermal cut of the plates (web and flange) and the flange-web welding [8,12,16]

The development of tensions at the flange tip shows that each effect has its own importance, and they must all be considered. Figure 2 also shows that EN 1993-1-14 [5] does not contain this effect, which might have to be modified.

2.2. Geometric Imperfections

Geometric imperfections are commonly associated with residual stresses that have been released, or that the object was not rigid enough to pin them. Every one of the stages of the production is also responsible for the strains that the object might form due to the deformation of the affected object.

The present investigation will consider the NP EN 1090-2 [9] so it can show which execution classes are relevant and if the elements respect the geometrical tolerances specified. Table 1 provides the web geometrical tolerances for the execution classes mentioned above.

Table 1 – Execution classes web geometrical tolerances [9]

Execution class	Quality	Máx. Imperfection
EXC1 e EXC2	D - EN ISO 5817:2015	$h_w/100$
EXC3 e EXC4	B/B+ - EN ISO 5817:2015	$h_w/150$

2.3. FEM modelling

The finite elements method used has two components, one is the thermal analysis and the other is the mechanical analysis.

For the thermal analysis the main equation used is:

$$c\dot{T} + kT = f_t \qquad (1)$$

This equation is the transient transfer equation, and the main parameter is the nodal temperature [19].

The mechanical analysis uses the values from the thermal analysis to compute the extension of the elements and the equations used are the compatibility equations.

3. Production geometry

3.1 Geometric and mechanical characteristics

As mentioned the current study is bases on the results of the production of 8 beams, which are organized in group A and group B. The focus will be on the values from 2 beams of the group B, which dimensions are listed and represented below.

Welded Section Beam G07 e G08		
L	3000	mm
h_w	830	mm
t_w	4	mm
a	1245	mm
h_w/t_w	207.5	-
a/h_w	1.5	-
$b_{fl,1} = b_{fl,2}$	300	mm
$t_{fl,1} = t_{fl,2}$	15	mm
b_{fl}/t_{fl}	20.0	mm
$Material$	S355	MPa

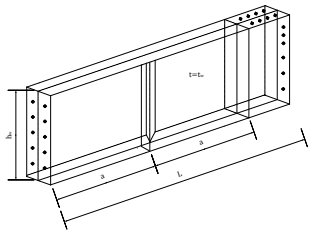

Figure 4– Geometric properties of the beams from the group B

These beams are created from an initial beam of 6000 mm length, which was cut in half to produce G07 and G08 plate girders (Figure 5).

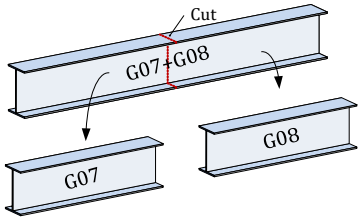

Figure 5– Cutting process of the beams from group B

The material used in the production of these beams is the S355JR, which properties were determined through the tensile tests [10].

3.2 Summary of the procedures

The procedures are to be summarized in 4 stages:

- ✓ Thermal cutting of the plates that will be used as flange and web
- ✓ Welding of the flange-web joint
- ✓ Cutting of the beam as represented in Figure 5
- ✓ Welding of the transverse stiffeners

For each stage several measurements are associated, those measurements are listed in Table 2. In these stages was also measured the voltage, amperage, and the time consumed by each process. These values are listed in Table 3, where is showed

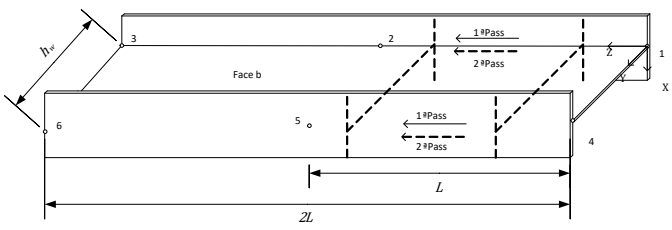

Figure 3 – Definition of the global axis of the beam in the welding flange-web stage

the velocity of the welding process and the respective energetic consumption.

Table 2 - Physical quantities measured in each stage of the production

Physical Quantities	Equipment	Work
Distance (mm)	Laser scan	Plasma cut (web, flange and transverse stiffeners)
Distance (mm)	Laser scan	Welding flange-web joint (submerged arc welding)
Extensions (%) + Distance (mm)	Strain Gauges + Laser scan	FICEP (cut)
Temperatures (ºC)	Thermocouples	Transverse stiffeners welding (MIG/MAG)
Temperatures (ºC)	Thermocouples	Other welding jobs (MIG/MAG)

Table 3 – Velocity and energetic consumption of the welding process

Welding process (G07+G08)				
Type	I[A]	U [V]	Average Velocity [mm/ min]	Bead
Submerged arc	300	24	1ª p. – 550 2ª p. – 595	Fillet a=3 mm

3.3 production stages

The plate thermal cutting process (arc of plasma) had the duration of approximately five and a half minutes, for a perimeter of 13660 mm results in an average velocity of 2484 mm/min (about 5 times bigger than the velocity of the process used for the plates of the group A, in which was used the oxycut process), such information is summarized in Table 4.

Table 4 – Comparation of the velocity between two types of cutting process used in the two groups of beams

Group of Beams	Web cutting process	
	Type	Aver. velocity (mm/min)
A (G01+G02)	Oxycut	493
B (G07+G08)	Arc of Plasma	2484

Generally, the oxycut process is much slower than the arc of plasma. It has other disadvantages, such as: working with lower temperatures; has less precision. However, it is considered a cheaper process and much simpler, so it's use is justified for several applications.

3.3.1 Plates thermal cutting

3.3.1.1 Web plate thermal cutting

In Figure 6 it is represented the generic conception of the cutting process, it's important to emphasize that is expected that during this process several relevant deformations will emerge in the plate, this deformations will be an amplification of the initial imperfections that were in the plate due to previous events.

Plate deformations measurements due to the cutting process were made through the point cloud capturing made by Laser scan (this equipment pick several points from the surroundings, using a "phase shift approach", and storage them for further analysis). After picking the information of each point, firstly all the values were corrected and simplified using a data treatment software to filter and smooth the points cloud. Finally, some images were created with a friendly MATLAB interface (Figures 6 and 7).

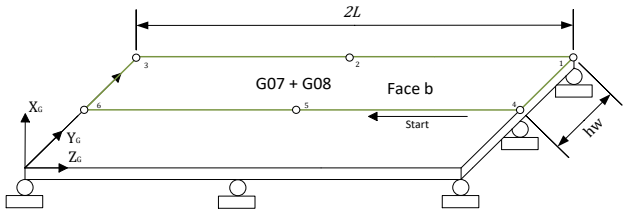

Figure 6 - Definition of the global axis of the plate in the cutting stage of the process (t_w=4mm)

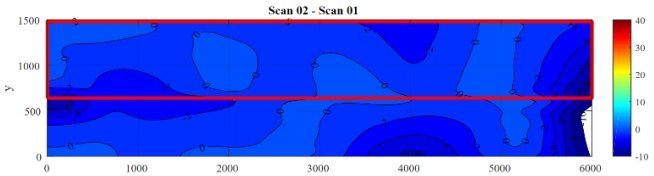

Figure 7 – Variation of the plate deformations with the arc of plasma thermal cutting in the web of beams G07+G08 (t_w=4mm)

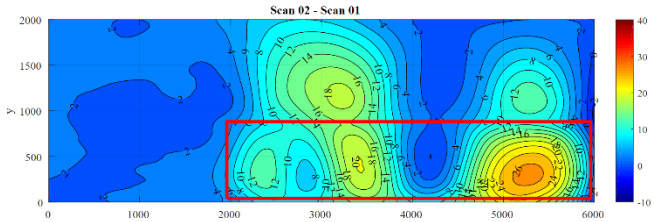

Figure 8 – Variation of the plate deformation with the oxycut thermal cutting in the web of beams G01+G02 (t_w=4mm)

The values of the imperfections were obtained 20 minutes after the end of the cutting process, for the thermal cut that used the arc of plasma the values of imperfections are quite smaller, and they were associated with the fact that this process is fast and with a very high cutting temperature. In fact, the higher value of speed and temperature makes the gradient of temperatures smaller, which leads to less relevant impact on the deformations of the plate [3].

For the Oxycut thermal process the conclusions are the same, but with the opposite reasoning. Since it works with smaller speeds and smaller temperatures the gradient of temperatures throughout the plate are bigger.

3.3.1.2 Flange plate thermal cutting

For the plates that will form the flanges of the beam, the thermal cut used was arc of plasma, these elements have a thickness of 15 mm which can mean that the deformations will be smaller. However, it is expected that in these elements, if it was used an oxycut thermal process, the element could have relevant deformations.

3.3.1.2 Transverse stiffeners plate thermal cutting

The stiffener plates were cut using the arc of plasma process, the thickness of this elements varies between 4mm, 6mm and 10mm.

3.3.2 Flange-to-web welding

The flange-to-web welding was executed with a submerged arc process, and the velocity, and energy consume are written in Table 3. In the **Erro! A origem da referência não foi encontrada.** i

s shown the global axis, and the position of the elements during the process.

To place each plate in the right position there were used several tools to fix those elements. Usually, to initially fix the plates together some heated drops of the filler metal used in the welding process are left in the beam with a specific spacing, these drops are used to fix some zones of plates together, so the welding process will be easier and more precise. Some clamps are used also in this process, to avoid the flange rotation during the welding process. In this stage of the production the deformations of the web were also captured through the same process that was described for the thermal cutting stage. Figure 9 to Figure 11 give the web plate deformed shapes for several stages.

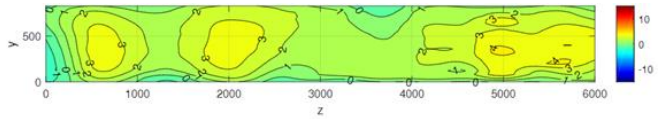

Figure 9 – Initial deformations field on the web before the welding process but after dropping metal fill and clamping the flanges (t_w=4mm)

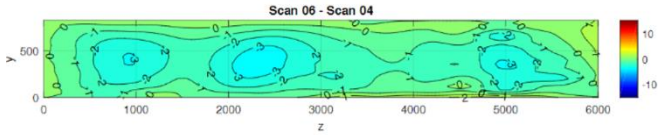

Figure 10 – Variation of the web plate deformations with the welding process (t_w=4mm)

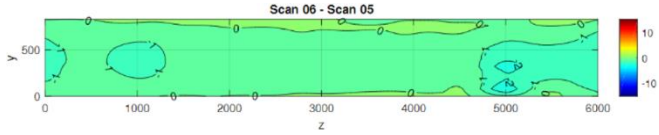

Figure 11 – Variation of the web plate deformations with the removing of the clamps (t_w=4mm)

The flange-to-web welding phase is responsible for the correction of some deformations that emerged in the thermal cut stage, in fact, in Figure 9 it is shown that all deformations in the plate edges are almost null, this is clearly different from the deformations that were captured after the thermal cutting of this element.

Figure 10 confirms that the new deformations due to the flange-to-web welding correspond to an amplification of the deformations that were established in the plate before this process.

3.3.3 PRS beam cutting

After the cutting and welding processes are completed, several residual stresses and deformations are contained in the plate girder. This stresses and strains will be released after their liberation when the beam is cut in half.

To capture the values of the strain and stress release, there were used several strain gauges, and their position is represented in Figure 12. The total duration of the cutting process took 15

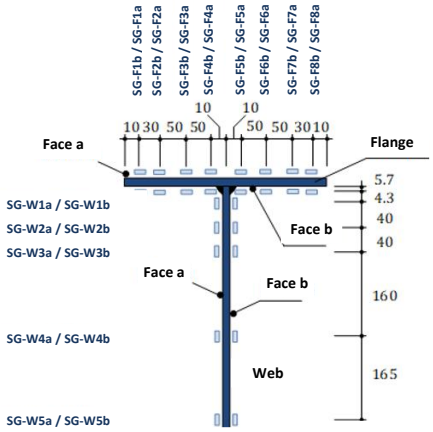

Figure 12 – Position of the strain gauges in the upper half of the beam

minutes, the strain values were taken from the strain gauges 25 minutes after finishing that time.

The method used to get the strains were the sectioning method, which consists in affecting the strain registered in on strain-gauge to a slice of the element that is being studied. This is a simplification, but it leads to some important results.

As it was expected, tension stresses emerged near the heated zone, and compressive stresses in zones farther from the action source. This has to do with the fact that the cooling of the material is not homogeneous throughout the beam.

The cutting of the beam did also introduce some, out of the web plane deformations that were captured with the Laser Scan (Figures 14 and 15). Some compatibility deformations were formed in the left edge of the web from the G07 beam and the right edge of the web from the G08 beam.

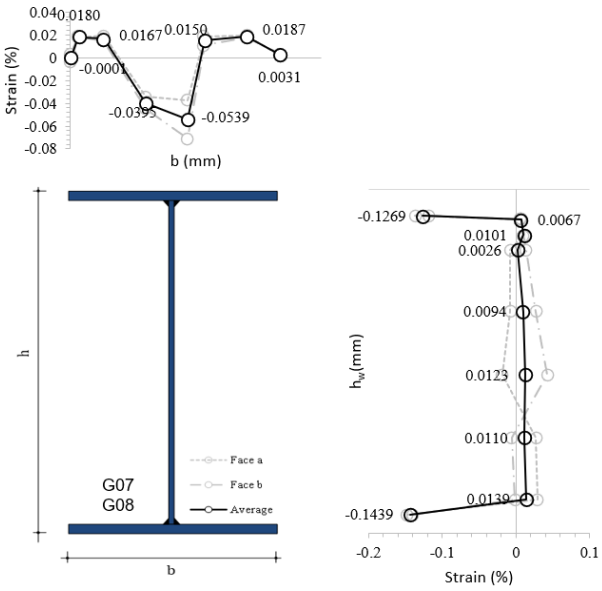

a)

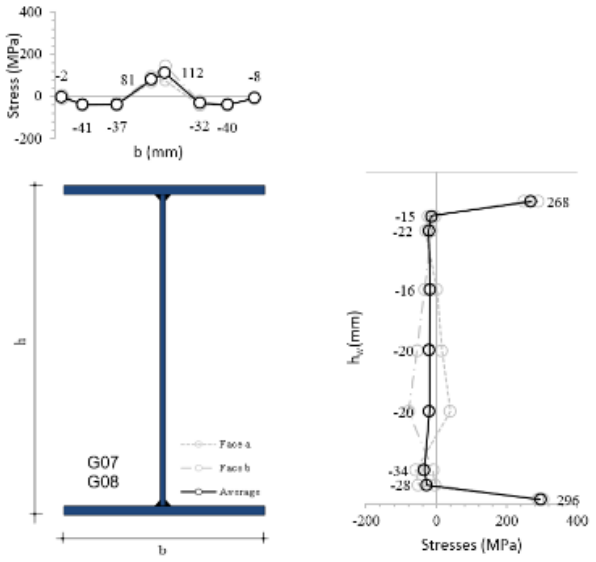

b)

Figure 13 – a) Strains measured in the strain-gauges, and b) stresses computed through the sectioning method [13]

Through Figures 14 and 15 deformations, it can be seen that this stage of the production is very important in the deformation's history of the web, in fact, this is the step that shows what effects did the welding and thermal cutting procedure combined turn up, in terms of residual mechanical

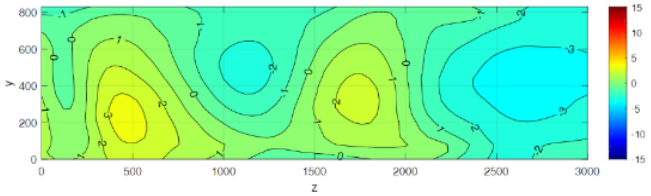

Figure 14 –Final deformations of the web of G07 beam after cutting the main beam (t_w=4mm)

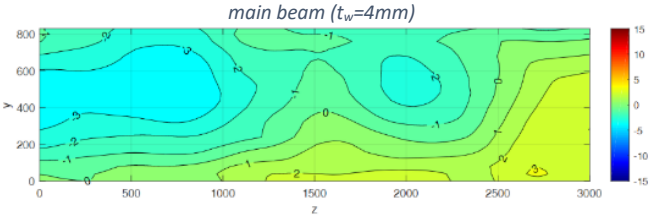

Figure 15 –Final deformations of the web of G08 beam after cutting the main beam (t_w=4mm)

variables in the beam.

3.3.4 Transverse stiffeners welding

The transverse stiffeners welding is the last relevant thermal step before these beams can be loaded. This is a stage where all final corrections must be made, so it can have a response to the mechanical loads that can be accurately modelled in an appropriated FEM model. Figure 16 shows the geometry of the transverse stiffeners and all the measurement devices used t this stage. In this step of the production the deformations of the web where also registered by the laser scan and the final values are represented in the Figure 17 and Figure 18.

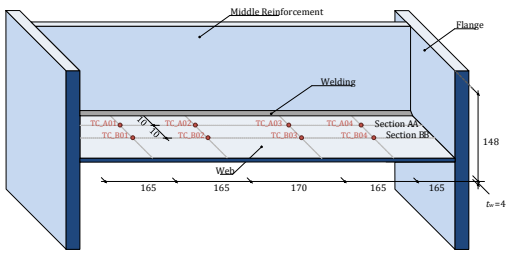

Figure 16 – Definition of the global axis of the beam in the stiffener welding stage and position of the thermocouples in the web

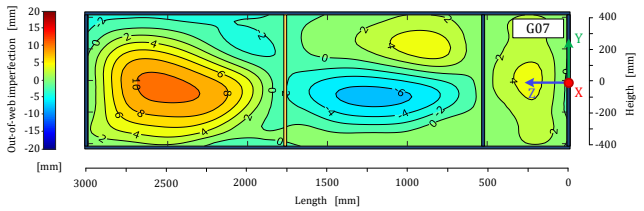

Figure 17 – Web imperfections in the beam G07 after transverse stiffeners welding

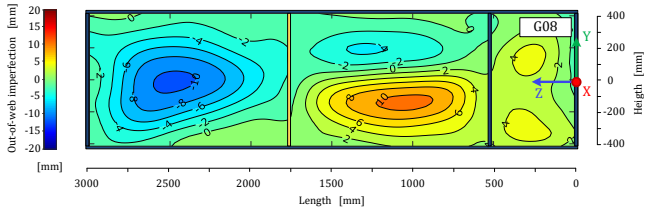

Figure 18 – Web imperfections in the beam G08 after transverse stiffeners welding

These deformations as it can be seen in Figures 17 and 18 are small in the zone where the transverse stiffeners have been welded and quite high in the centre of each panel. Another observation is related with the sign of the deformations, in fact, if one of the panels have a positive deformation, the other has the opposite sign, this means that the transverse stiffeners are not rigid enough to block the rotations of the web. The panel with a smaller span has register, as predicted smaller deformations.

3.4 Discussion of the results

One of the advantages of welded plate girders is the resistance capability they have despite the high slenderness of its elements. However, those elements must be treated with special attention, since the mechanical models that are used to predict their behaviour, when applied to the structure, depends on the relevance in the residual imperfections.

Beginning to look to the results of the first stage, i.e., the imperfections that result of the thermal cutting. It can be concluded that this stage has a strong impact on the deformations of the plates. The fact that these plates are thin and almost free to deform shows that this step could lead to almost 10 mm deformations, due to the thermal cut using the arc of plasma. If the process is accomplished with oxycut the results are much higher leading to a deformation peak variation of almost 26 mm. This has to do with the characteristics of each type of thermal cut.

In fact, if this was the only process to consider, the conclusion could be that the arc of plasma process is better, and it should be the one used on this kind of plates, with smaller thickness. However, the existence of the other production stages lead to further conclusion. The second stage, relates to the flange-to-web welding. At this stage the displacements are small and the fact that the web edges that will be welded are fixed in a position with a null value of initial deformation shows that this step has a corrective effect. As it can be seen this step leads to displacements much smaller than the previous one, the peak variation value is about 0.3 cm.

It is important to refer that since this step might have a lower deformation but some other effects, like residual stress, much have increased in this step, since this is no longer a simple plate but the convergence of 3 plates (two flanges and one web), with different geometries.

This conclusion could be checked in the next stage of the production, in fact the cold cutting of the PRS beam showed exactly the development of the residual stresses field. The residual stresses field show tension values in the welding region and compression values far from this region. Yet, beams G07 and G08 show compression residual stresses in flanges tips while for group A beams and from the study reported in [8,12,16], tension was reported (Figure 19). In fact, this fact is related with the type of thermal cut used on the flange's plates. For the plates of the beams G07 and G08 the thermal cut used was the arc of plasma (see Figure 13), for the other beams it was used oxycut. This means that the cut process affects the type of residual stresses obtained at the flange tips. In terms of deformation, the web, shows at this stage small values of peak deformation, reaching final peak values of 3mm near the cut section. At this point, it was possible to understand how the history of deformations changes throughout the beam production and highlights the more significant steps in terms of geometric deformations. At this point, it was possible to understand how the history of deformations changes throughout the beam production and highlights the more significant steps in terms of geometric deformations. Calling stage 1 to the initial time, 2 to the end of the thermal cutting process, 3 to the end of the welding process and 4 to the end of the cold cutting of the PRS beam process, it's possible to relate the deformations of each step to the limits of deformations imposed by NP EN 1990-2 [9] (Figure 20).

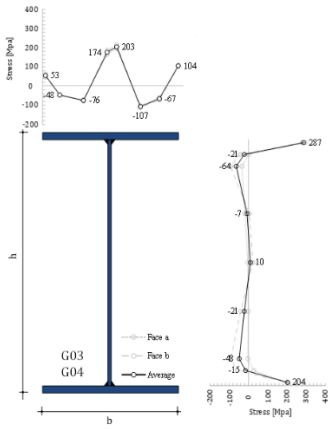

Figure 19 – Results of the beams G03+G04 (group A) and of the beams studied by "Universidade de Coimbra"

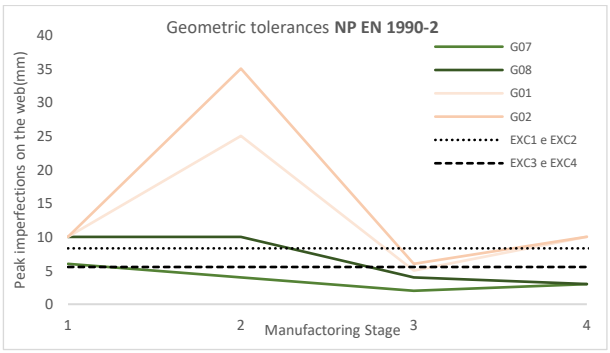

Figure 20 – Comparing peak deformations of the web in the beams G01+G02 and G07+G08 with the defined limits in the NP EN 1990-2 [9]

Through the values represented above, for beams G07 and G08 the peak values converge to a final value within the limits defined in the norm. For group A beams (G01 and G02) the values are dispersed in each stage. In the thermal cutting process, the values reach a peak of 35 mm, in the welding process they reach 6 mm, which has to do with the corrective component of this stage. After stage 4 the values are out of the limits defined, this shows the impact of the initial cutting process in this stage.

The fact that the beams G01 and G02 do not fulfil the norm requirements at this stage does not mean that they can't be used, it just means that they need to have another corrective stage. In this case, that stage is the welding of the transverse stiffeners, which have mainly a structural purpose, but it also might help to achieve a better imperfection value.

Table 5 lists the final imperfections on each web panel after the welding of the transverse stiffeners for all groups of beams.

Table 5 – Final peak values of deformation at each web panel

Final warpage of the web after the reinforcements welding				
Girder	Left panel [mm]		Right panel [mm]	
	Max.| Min		Max.| Min	
G01	+5.51 | -7.13	h_w/116	+4.04 | -7.26	h_w/114
G02	+5.14 | -11.80	h_w/70	+9.17 | -0.28	h_w/91
G03	+10.49 | -4.54	h_w/79	+3.78 | -5.66	h_w/147
G04	+5.06 | -5.36	h_w/155	+7.49 | -1.50	h_w/111
G05	+11.16 | -3.06	h_w/74	+6.78 | -4.73	h_w/122
G06	+3.51 | -8.31	h_w/100	+2.48 | -5.66	h_w/147
G07	+10.71 | -2.76	h_w/78	+5.40 | -6.89	h_w/120
G08	+1.48 | -10.48	h_w/79	+10.71 | -4.30	h_w/78

These results show that the final imperfections are not, necessarily, better in the plates where the cutting process was the arc of plasma. This is a step that has lots of corrective actions that makes the deformations introduced by previous stages irrelevant. However, it is not irrelevant in a time waste perspective. In fact, it's expected that in the web plates where the thermal cut used was oxycut the time waste in corrective measures is quite high, since the deformations that came from previous stages are much higher. These values of deformation are quite important since they will be used in loading tests.

4. FEM of the Flange-to-Web Welding

4.1 Model Calibration

The need for modelling the welding flange-to-web joint comes by the fact that in the real process some of the thermal effects are not easily understandable. The main purpose of this model is to get similar results to the ones reported in production measurements and find a way to reproduce them separately.

The type of analysis used in this model was GMNA, which means that the geometric and material properties are nonlinear, and it was done with the support of AWI (Abaqus welding interface [7,19]). The work was divided in three steps:

- Geometric and Mechanical Modelling
- Analysis [8]
- Validation and Verification [16-19]

Geometric and Mechanical Modelling – In these step two parts were formed and the material was assigned to each of those parts. A solid extrusion part with a T-shape section and with the transversal dimensions of one half of the PRS beam, since it was adopted a symmetry simplification, and with a length of 500mm (simulating the PRS beam), and two solid extrusion parts with a triangular cross sections shape with 500 mm length (simulating the welding fill).

The material proprieties used are listed in Table 6. These values are only valid while the steel temperature is about 21°C. In fact, when the welding process starts these parameters change. The mechanical ones suffer a degradation, the thermal ones, with the increasing of temperature they have different behaviours. All that information can be checked in Table 7.

Table 6 – Mechanical and thermal parameters of steel at initial room temperature

Mechanical Properties					
Aço	f_y (MPa)	f_u (MPa)	E (MPa)	Density (ton/mm^3)	Poisson Coef.
S355	355	490	210000	7.85E-09	0.3
Thermal Propreties					
α (/°C)	C_{spe} (cal.ton^{-1}.°C^{-1})	Cc_{ond} (mW/mm.K)	Latent Heat (°C)	Liquidos Temp (°C)	Solidus Temp (°C)
1.20E-05	440000000	53.3	2600	1390	1340

Table 7 – Mechanical and thermal parameters variation with the temperature increasing [6,21]

Θ	$k_{fy,\Theta}$	$k_{fp,\Theta}$	$k_{E,\Theta}$	$C_{exten,\Theta}$	$C_{spc,\Theta}$	$Cc_{ond,\Theta}$
20	1.000	1.000	1.000	1.20E-05	402457143	54.3
100	1.000	1.000	1.000	1.21E-05	460285714	51.3
200	0.807	1.000	0.905	1.23E-05	532571429	47.6
300	0.613	1.000	0.800	1.24E-05	604857143	43.9
400	0.420	1.000	0.700	1.26E-05	677142857	40.1
500	0.360	0.780	0.600	1.27E-05	749428571	36.4
600	0.180	0.470	0.310	1.28E-05	821714286	32.7
700	0.075	0.230	0.130	1.30E-05	894000000	29.0
800	0.050	0.110	0.090	1.31E-05	922000000	25.4
900	0.038	0.060	0.068	1.32E-05	623830508	26.3
1000	0.025	0.040	0.045	1.34E-05	658406780	27.1
1100	0.013	0.009	0.023	1.35E-05	692983051	28.0
1200	0.013	0.009	0.022	1.37E-05	727559322	28.8
1450	0.013	0.009	0.019	1.40E-05	814000000	31.0
1500	0.013	0.009	0.019	1.40E-05	814000000	110.0
3000	0.013	0.009	0.005	1.40E-05	814000000	110.0
(°C)	-	-	-	m/m	mJ/(ton.K)	mJ/(mm.s.K)

Analysis – This step is responsible for the definition and verification of the mesh and of the interactions.

The elements to use in the definition of the mesh where, DC3D8 in the case of the thermal analysis, and C3D8R for the mechanical analysis. Both the elements are geometrically similar, i.e., both are formed by hexahedrons with 8 vertices and 6 edges, however, in the case of the DC3D8 the vertices are also the integration nodes, in the case of C3D8R the vertices are points where we can get interpolated information, the integration node is only one and is in the centre o the element. Another difference is related with the degrees of freedom, in the case of the thermal analysis it is used 1 DOF per node (temperature), in the case of the mechanical analysis it is used 3 DOF per node (three orthogonal displacements).

The mesh spacing is defined by the criterion $e_{spa}=h_w/60$, which resulted in a mesh with 5 mm spacing. The mesh density is not homogeneous along all the beam, it is used a more refined mesh near the welding zona and a less refined mesh in the farther zones. All this information is represented in the Figure 21.

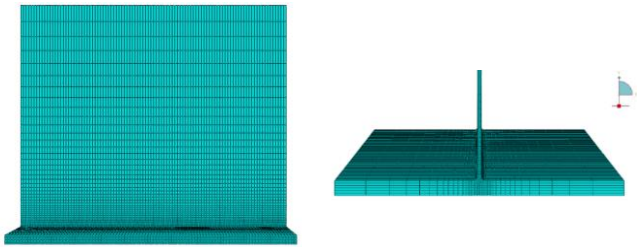

Figure 21 – Mesh definition with a minimum spacing of 5 mm, near the welding zone, and a maximum spacing of 50 mm

After the mesh definition is important to set the boundary conditions and the time of each step. In the case of the welding process model, we will have 11 boundary conditions, 8 in the flange, and 3 in the web, to consider the symmetry simplification. Figure 22 shows all the information that is needed to define the analysis process.

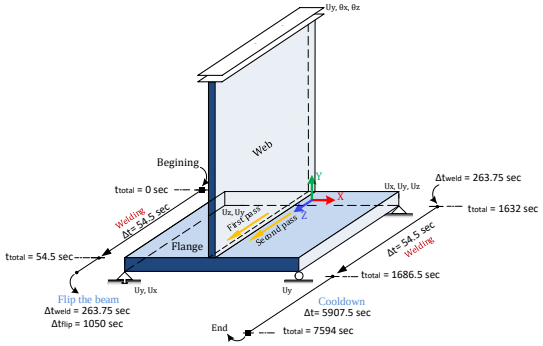

Figure 22 – Boundary conditions and the chronology of the model

With this information it is possible to use the AWI plugin to create the rest of the interactions, however, it is important to refer the simplifications that will be considered. The first is related with the velocity and temperature of the welding, in this model it will be considered that both those variables are constant in time. The second is related with the mechanical boundary conditions, it is assumed that those BC don't have a relevant impact on the results. The last one is related with the room temperature: It is assumed that the temperature is constant, and the value is 21.1°C. Tables 8 and 9 list the relevant parameters used in the analysis.

Table 8 – Mechanical and thermal parameters introduced in the AWI

Initial Geometry and Thermo-Mechanical Properties					
Nome da Parte	Sistema de Unidades	Material Base	Temperatura Inicial (°C)	Constante de Stefan-Boltzmann (mJ/s/mm^2/K^4)	Zero Absoluto
"Viga + Soldadura"	SI	S355	21.1	5.67E-11	-273.15
Propriedades Mecânicas e Térmicas Impostas					
Material da Soldadura	Temperatura liquidificação do aço de solda (°C)		Temperatura do aço de solda (°C)		
S355	1995		2000		

Table 9 – Values of each step associated to each chunk*

"Pass Control"			
Time Period (s)	Initial time increment (s)	Minimum time increment (s)	Máximum time incremen
0.5	0.01	1.00E-07	0.1
Máximum number of increments	Máximum allowed temperature change (°C)	Film Coeficient (mJ/s/mm^2/K)	Emissivity
1000	250	0.025	0.9

*Chunk: Small portion of all the weld bead used in the model

Is important to explain that the welding model does not use a continuous torch that simulates the process, instead the process is simulated with small chunks that are deposited in the base material at the temperature defined by the modeller. In this case the temperature used was 2000°C (see Table 9). Usually, the size of those chunks is determined by the mesh spacing.

4.2 Relevant outputs

One of the most important information that as to be read in the model is the duration of the analysis and the number of elements used, this is what shows the yield of the model. In Table 10 and in Table 11 those values can be checked.

Table 10 – Relevant values from the thermal analysis performance

Thermal analysis preformance- Welding		
User time (s)	CPU time (s)	Nº elements
29836	30449	28400
Nº nodes	Nº of degrees of freedom	Elements type
35754	35754	DC3D8 (3D 8-node linear isoparametric element)

Table 11 – Relevant values from the mechanical analysis performance

Mechanical analysis preformance- Welding		
User time (s)	CPU time (s)	Nº elements
17936	18534	28400
Nº nodes	Nº of degrees of freedom	Elements type
35754	107262	C3D8R (3D 8-node linear isoparametric element*)

4.3 Results

4.3.1 Thermal analysis results

In the thermal analysis some values must be according with the experimental ones. For that purpose, some nodes in the model were used to get thermal information, and the position of those nodes coincide with the position of thermocouples used in the experimental analysis. Those results can be observed in Figure 23 for the flange, and in Figure 24 the for the web.

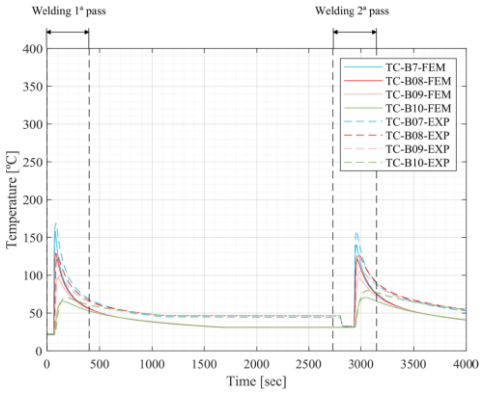

Figure 23 – In the left Figure are represented the model temperature values, in the right the values captured by the thermocouples (t_{fl}=15 mm)

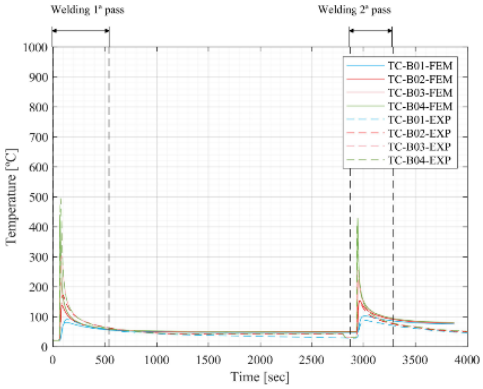

Figure 24 – In the left Figure are represented the model temperature values, in the right the values captured by the thermocouples (t_w=4 mm)

Figures 23 and 24 show that the thermal modelling is apparently quite accurate, the peak values of the model are very close to the experimental ones and the graphics format is quite similar. However, However it should be noticed that some differences should be seen since the model is a discrete process and the reality is almost continuous. Also, the material properties defined by Pilipenko [21] are different from the real ones.

4.3.2 Mechanical analysis results

After concluding the thermal analysis, the temperature information is used as a predefined field on the mechanical model. Through the expansion coefficient and the mechanical properties of the material stresses and strains will emerge in the model. The referential used in this part of the work is (1,2,3) and this axis are the same (X,Y,Z) used in the modelling stage.

In terms of residual stress the relevant information is the stress according to the "Z" axis, and the relevant values, to be compared with the experimental ones, can be interpolated linearly by the values caught on the integration nodes near the position of the stain-gauges defined in 3.3.3. The comparison between experimental results and FEM residual stresses are given in Figures 25 and 26, for the flange and the web.

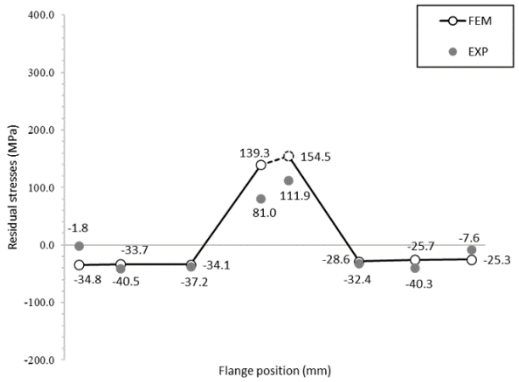

Figure 25 – Residual stresses in the section midline got in the FEM model on the flange and the experimental results (t_{fl}=15 mm)

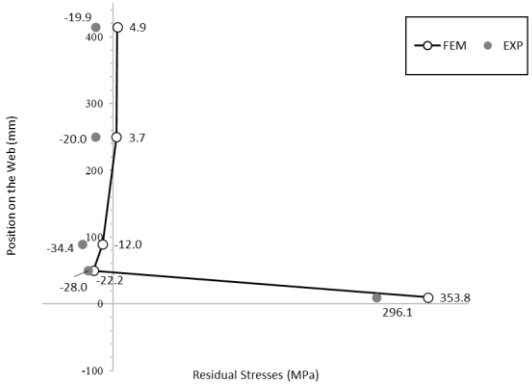

Figure 26 – Residual stresses in the section midline got in the FEM model on the web and the experimental results (t_w=4 mm)

In terms of midline stress results the experimental values and the FEM values are quite comparable. The small differences that can be spotted are related with the fact that the effect of the thermal cut of the plates it is not considered. In fact, it is predictable that the thermal cut of the flange plate will introduce compressions in the mid zone of the plate and tensions in the edges, what will make the difference between the values above even smaller. For the web, the same type of result will occur since the compressions in the mid zone of the web will also bring the experimental and FEM values closer together.

4.3.3 Stresses history

In this stage of the work the residual stresses and strains were analysed in 3 elements. These elements were chosen according to the position of the strain-gauges SG-W1a, SG-F6a and SG-F6b.

In the element SG-W1a the strain-stress values show what is the path that is being followed during the welding process (Figure 27).

It is possible to conclude that, even without any temperature increase the element is already deforming and developing some compression stresses, this must do with the fact that other elements, near this one, are already feeling some effect, forcing this element to react. When temperature starts to increase in this element, rapidly he outruns the yielding stress causing its plastification, due to the high compression stresses that emerge in the element. At the end of the heating stage, this element, has a large value of compression strain and a small value of stress, since its rigidity is reduced.

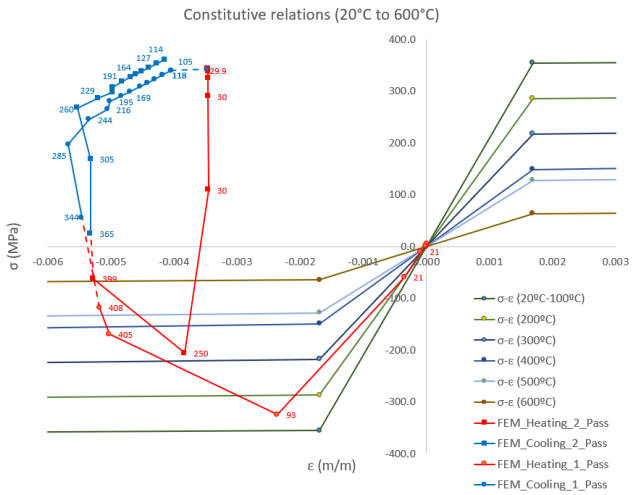

Figure 27 – Strain-Stress path followed by the element during the welding process (t_w = 4 mm)

The colling stage shows the impact of the rigidity regeneration. In fact, the values of strain are settled and, since the cooling is quick, the element is rigidity quickly grows and keeps the element with the same values of deformation, however, the values of stress became positive, since the object wants to retract but the elements nearby are blocking it.

One important aspect that this study shows is that the reheating of the element leads to similar residual stresses when compared with the values from the first heating, at least for elements near the heat source. In fact, this can justify that when an element is reheated the residual stresses are not duplicated, but in fact it might be closer to the stress average.

For elements SG-F6a and SG-F6b the strain-stress path are quite different than the one represented above, comparing Figure 27 and Figure 28 those differences can be checked. Through these results it is clear that there is no plastification of the element. It is also possible to see that an average hypothesis to consider the reheating action is not so accurate for this element. The fact that the results are quite different in the first welding pass and in the second welding pass indicate that for this case assuming a superimposition of effects might be more accurate.

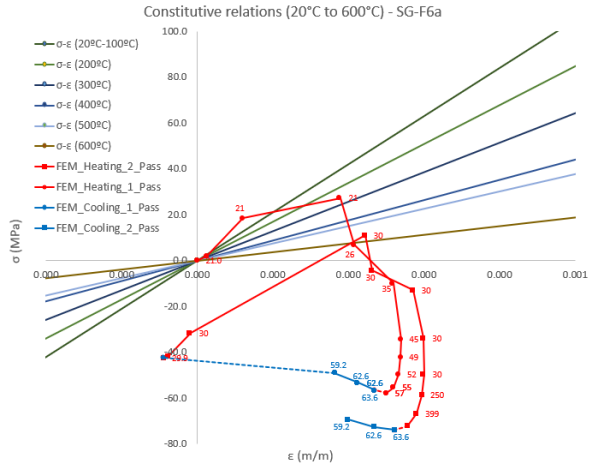

Figure 28 – Strain-Stress path followed by element SG-F6a during the welding process (t_{fl} = 15 mm)

4.4 Discussion of the Results

Through the model results it can be concluded that the welding stage is responsible for most of the stresses introduced in the plates. In fact, the experimental and the FEM results are quite similar, despite the small differences due to the isolated modelling of the process, i.e., without considering the values that emerged in the thermal cut of those plates.

This modelling was also useful to determine the influence of each thermal process in the final residual stresses. It is possible to conclude that there should be two ways to add the values from each effect. One is by an average hypothesis, if the zone that is being analysed is near the thermal source, and the other is through the sum of each effect, if the zone is farther away.

5. FEM of the thermal cutting

5.1 Model Calibration

The model calibration is quite the same that was used to study the welding process, differing only on the number and in the time of the steps, and on the boundary conditions (Figure 29).

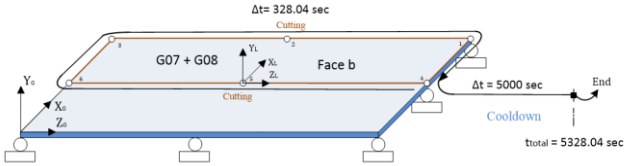

Figure 29 – Boundary conditions and the chronology of the model

Conceptually the model is very similar the previous one, however, instead of external elements that represent a material fill we will have internal elements that represent the material destruction, through their removal.

5.2 Results

5.2.1 Mechanical analysis results

In terms of residual stresses, there are only small differences between these values and the experimental values (Figure 30).

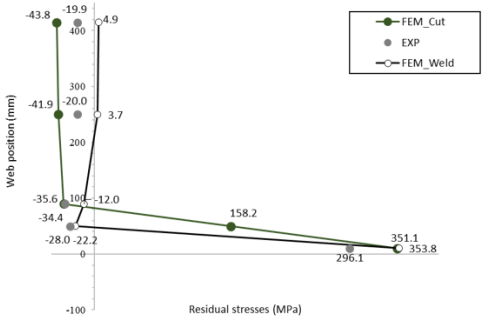

Figure 30 – Comparation between the cutting model residual stresses and the experimental values.

The fact that the cutting model gave results very similar to the welding model is because the application point and the thermal characteristics are the similar for the two actions. In fact, if an average hypothesis is considered to add the two effects introduced by the thermal actions the results will be quite the same as the ones captured experimentally. This can be justified by the fact that the web plate thickness is very low, and, for that reason, all the web plate area can be considered as a zone near the heating source (see 4.4.).

6. General Conclusions and Further Developments

The results from the experimental work show that the arc of plasma thermal cut is much smother then the oxycut process, however this does not mean that it is always the best cutting process, since the differences between the deformations became small when the welding of the transverse stiffeners take place. In fact, one parameter that should be studied is the time dispended

on the correction of the plate deformations, before welding those plates.

However, the flange plates deformations cannot be easily corrected in the welding transverse stiffeners phase, which makes the final values of residual stresses and deformations highly dependent on the thermal cutting process. The Eurocode 3 does not differentiate the residual stresses diagram shape with the thermal process used, however, it has been found that the differences are not irrelevant, which could justify an update of the proposed residual stress patterns for special cases.

In terms of FEM modelling the values got in the welding process modelling are close to the experimental ones, which means that most of the residual stresses are directly associated with this process. The thermal cutting process also introduced similar values to the welding process in the web, but since the two processes have the thermal source applied in the same zone this means that in fact the process can be seen as a reheating process.

The fact that the process is a repetitive and the residual stress values quite similar can justify the conclusion that their values can be combined through a stress average.

Other information, such as the residual stresses in the flange tips for each process showed that another type of combination must be used for this zone, such as a superimposition of effects.

One important future development is related with the combined modelling of all the effects, this is, the creation of a FE model that, in a first stage simulates the thermal cutting of the flange plate, in a second stage the thermal cutting of the web, and, in a last stage the welding of the plates. Such a model will provide a global view of the combined results of the residual stresses and will be a way to evaluate the stress superposition thesis proposed in this research.

7. Notation

b_{fl}	Flange width
$t_{fl,i}$	Thickness of the flange i
h_w	Clear web depth between flanges
t_w	Thickness of the web
c	Heat capacity of the material
$\dot{T}$	Derivation in time of the nodal temperature
k	Thermal conductivity of the material
T	Nodal Temperature
f_t	Thermal flux
L	Total length
a_s	Welding fillet
I	Voltage
A	Amperage
X_G, Y_G, Z_G	Global axis
f_y	Yield strength
f_u	Ultimate strength
E	Young's Modulus of structural steel
α	Coefficient of thermal expansion
$C_{spe.}$	Specific heat
$C_{cond.}$	Thermal conductivity
$k_{fy,\theta}$	Reduction factor of the yielding strength
$k_{fp,\theta}$	Reduction factor of the ultimate strength
$k_{E,\theta}$	Reduction factor of the young's modulus
DOF	Degrees of freedom
e_{spa}	Mesh spacing
FEM	Finite element method
EXP	Experimental values

8. References

[1] Oliveira Pedro; José, Mendes, Pedro (2020) Dimensionamento de Estruturas de Edifícios e Estruturas Especiais | 2 Volumes. IST Press.

[2] Jenney, Cynthia; O'Brien, Annette (2001) Welding Handbook: Welding Science and Technology (9thEdition). American Welding Society.

[3] Oliveira Santos, José; Quintino, Luísa (1998) Processos de Soldadura. Instituto de Soldadura e Qualidade.

[4] Macherauch, Eckard (1987) ADVANCES IN SURFACE TREATMENTS. VOLUME 4 – International Guidebook on Residual Stresses. A NIKU-LARI in cooperation with the Institute for industrial technology transfer.

[5] CEN (2010), EN 1993-1-1, 2005, Eurocode 3: Design of Steel Structures - Part 1-1 General rules and rules for buildings, European Committee for Standardization, Brussels.

[6] CEN (2010) EN 1993-2, 2010, Eurocode 3: Design of Steel Structures - Part 1-2 General rules – Structural Fire Design, European Committee for Standardization, Brussels.

[7] CEN (2010) EN 1993-2, 2010, Eurocode 3: Design of Steel Structures - Part 1-5 Design of steel structures – Part 1-5: Plated Structural Elements, European Committee for Standardization, Brussels

[8] CEN (2010) EN 1993-14, 2020, Eurocode 3: Design of Steel Structures - Part 1-14 General rules - Design assisted by finite element analysis, European Committee for Standardization, Brussels.

[9] CEN (2011), EN 1090-2, Execution of steel structures and Aluminium Structures. Part 2: Technical Requirements for Steel and Aluminium Structures, European Committee for Standardization, Brussels.

[10] CEN (2009), EN ISSO 6892-1, Mettalic-Materials – Tensile Testing. Part 1: Method of test at room temperature (ISO 6892-1:2009), European Committee for Standardization, Brussels.

[11] CEN (2001) EN 1011-2 2001, Welding Recommendations for welding of metallic materials. Part 2: Arc Welding of ferritic Steels, British Standard.

[12] European Convention for Constructional Steelwork (ECCS) – Technical Committee 8: Ultimate Limit State Calculation of Sway Frames with Rigid Joints, ECCSPublication No.33, Brussels, Belgium, 1984.

[13] N. Tebedge, G. Alpsten, L. Tall, Residual-stress Measurement by the Sectioning Method, 1973

[14] Mitra U and Eager T W 1991 Slag-Metal Reactions during Welding: Part I. Evaluation and Reassessment of Existing.

[15] Andersen, Leif. (2018) The need for Pre-Heating when Welding, TE Andersen Consulting.

[16] Schaper, Lukas. Tankoya, Trayana. Simões da Silva, Luís. Knobloch, Markus. (2022) A novel residual stress model for welded I-sections, Journal of Constructional Steel Research.

[17] Kollar, Dénes (2020), Welding Simulation in Advanced Manufacturing and Design of Steel Structures, Budapest University of Technology and Economics, Hungary.

[18] Gannon, L., Liu Y., Pegg N. and Smith, M. Effect of welding sequence on residual stress and distortion in flat-bar stiffened plates. Mar. Struct., 2010, 23, 385-404.

[19] Seleš K., Perić M. and Tonković Z. Numerical simulation of a welding process using a prescribed temperature approach. J. Constr. Steel Res., 2018, 145, 49-57.

[20] Yi M.S., Hyun C.M., Paik J.K. Full-Scale Measurements of welding-induced initial deflections and residual stresses in steel-stiffened plate structures. International Journal of Maritime Engineering – December 2021.

[21] Pilipenko, A. Computer simulation of residual stress and distortion of thick plates in multi electrode submerged arc welding. Norwegian University of Science and Technology – July 2001.